Biomaterials Advances 185 (2026) 214895

Contents lists available at ScienceDirect

Biomaterials Advances

journal homepage: www.journals.elsevier.com/materials-science-and-engineering-c

Plasma-sprayed 45S5-bioactive glass coating provides superior anti-biofilm activity compared to hydroxyapatite coating while maintaining host cell cytocompatibility and antibacterial immune activation

Elisabeth Seebach [a,b,*], Jan Philippe Kretzer [c], Therese Bormann [c], Jens Gibmeier [d], Robert Vaßen [e], Elke Kunisch [f], Tobias Renkawitz [g], Fabian Westhauser [g,**]

[a] Department of Infectious Diseases, Medical Microbiology and Hygiene, Medical Faculty Heidelberg, Heidelberg University, Heidelberg, Germany
[b] University Hospital Heidelberg, Heidelberg, Germany
[c] Research Center of Biomechanics and Implant Technology, Department of Orthopaedics, Heidelberg University Hospital, Heidelberg, Germany
[d] Karlsruhe Institute of Technology, Institute for Applied Materials (IAM-WK), Karlsruhe, Germany
[e] Forschungszentrum Jülich GmbH, Institute for Energy Materials and Devices (IMD-2), Jülich, Germany
[f] Research Centre for Molecular and Regenerative Orthopaedics, Department of Orthopaedics, Heidelberg University Hospital, Heidelberg, Germany
[g] Department of Orthopaedics, Regensburg University Medical Center, Bad Abbach, Germany

ARTICLE INFO

Keywords:
45S5-bioactive glass coating
Atmospheric plasma spraying
Mesenchymal stromal cells
Staphylococcus epidermidis
Biofilm formation
Macrophage immune response

ABSTRACT

Periprosthetic joint infections (PJIs) are a major complication in joint arthroplasty, leading to higher mortality, poorer outcomes, and increased failure rates in revision surgeries. Revision challenges include patient risk factors, bacterial resistance, and the need for implants that combine biological integration with antibacterial effects. The 45S5-bioactive glass (BG), with its unique osseointegration and antibacterial properties, shows promise over hydroxyapatite (HA), though its high-temperature crystallization limits the appropriate coating technologies. Using atmospheric plasma spraying (APS) with controlled thermal exposure, we successfully applied coatings of Ti-6Al-4V alloys with either HA or BG, while preserving bioactivity and mechanical properties of the BG coating. This study compared HA and BG coated Ti-6AI-4V discs in terms of cytocompatibility, effect on biofilm formation and macrophage immune response. In doing so, we demonstrated that both coatings showed comparable attachment and viability of human bone marrow stromal cells (BMSC). We found a significant reduction in biofilm formation of *Staphylococcus epidermidis* (SE) on the BG coatings, while a pro-inflammatory macrophage activation by bacterial colonization and biofilm formation was preserved. Overall, our study shows that BG exhibits the same properties as HA regarding BMSC attachment and survival, whereas it is superior regarding its anti-biofilm characteristics further allowing for macrophage immunocompetence against bacterial colonization. Therefore, incorporating BG coated implants into revision joint arthroplasty has the potential to enhance and advance current coating strategies by providing a multifunctional approach that combines osteoconductive and antibacterial properties.

1. Introduction

Periprosthetic joint infections (PJIs) constitute a major complication of total joint arthroplasty surgery [1]. Patients suffering from PJIs show not only a significantly increased one-year mortality but also poorer functional outcomes when compared to patients without PJI [2,3]. The most common mode of failure in revision arthroplasty are PJIs [4] – registry data shows that the risk for re-revision is doubled when the first revision surgery was performed due to PJI when compared to aseptic cases [5]. The possible reasons for failure of revision arthroplasty in PJIs are as varied as they are multifactorial [2,6]: in addition to the individual risk profile of the patients [6,7], factors such as the microbiological profile including bacterial resistance [8] or the extent of bone destruction [9] have a considerable influence on the results of revision operations. Nevertheless, it is also important to critically question the extent to which revision implant systems are capable of coping these

* Corresponding author at: Department of Infectious Diseases, Medical Microbiology and Hygiene, Medical Faculty Heidelberg, Heidelberg University, Germany.
** Corresponding author.
E-mail addresses: elisabeth.seebach@uni-heidelberg.de (E. Seebach), Fabian.Westhauser@klinik.uni-regensburg.de (F. Westhauser).

https://doi.org/10.1016/j.bioadv.2026.214895
Received 6 February 2026; Received in revised form 1 April 2026; Accepted 17 April 2026
Available online 20 April 2026

complex situations: an ideal revision implant would simultaneously anchor biologically and demonstrate local antibacterial efficacy.

In order to achieve these properties, remarkable efforts have been undertaken to functionalize implant surfaces following different approaches: (i) metal alloys can be structured to aggravate bacterial adhesion, (ii) metal surfaces can be coated or (iii) the metal alloys themselves can be doped using antibacterial agents [10–12]. A promising biomaterial that can be used to functionalize metal surfaces toward both, osseointegration and antibacterial activity is the 45S5-bioactive glass (BG) composition (in wt%: 45.0 SiO_2, 24.5 CaO, 24.5 Na_2O, 6.0 P_2O_5) [13]. BG was introduced in the late 1960s by Professor Larry Hench and is available for clinical use in orthopedic procedures for more than two decades [14]. The rapid exchange of ions on the BG surface leads eventually to the formation of a carbonated hydroxyapatite-layer on the surface – this mechanism, that defines the bioactivity of the material, does not only allow for a strong bonding of the BG to surrounding tissues and integration into the surrounding bone but also leads to the release of biologically active ions such as pro-osteogenic silicon [15,16]. Furthermore, besides its excellent regenerative properties in the treatment of bone defects, BG also acts bactericidal against a broad variety of bacterial strains [14,17–20]. The combination of these properties is unique and not met by other synthetic biomaterials that are used for surface functionalization of implants such as hydroxyapatite (HA).

However, despite these favorable properties, based on the strong initial exchange of ions, BG might develop conditions that hamper cell viability at least under in-vitro conditions [21]. Furthermore, BG crystallizes when treated with temperatures of around 600 °C which compromises its bioactivity and mechanical properties [22,23]. To preserve the bioactive properties of BG, which rely on the high reactivity of its amorphous structure, crystallization must be avoided. Therefore, when surfaces shall be functionalized with BG, coating protocols are needed that prevent prolonged exposure to high processing temperatures.

Although BG offers the prospect of combined osteogenic and antibacterial functionalization of implants, there is no BG coated implant for revision arthroplasty available for clinical application whilst HA coated revision implants are frequently used [24,25]. Furthermore, no directly comparative data is available comparing HA and BG coatings in terms of cytocompatibility, anti-biofilm activity and potential effects on antibacterial immune response. Therefore, it remains unknown whether BG could provide advantages over current state-of-the-art HA coatings in revision implant systems.

In this study, Ti-6Al-4V alloy discs were coated with HA or BG using atmospheric plasma spraying (APS), followed by morphological characterization. During APS, the glass powder particles are injected into a high-temperature plasma flame. During the residence time of the glass particles in the flame, they will be accelerated and molten. Furthermore, upon impact on the substrate, the molten droplets experience rapid cooling (quenching), preventing crystallization and ensuring that the deposited BG remains amorphous [26,27]. Both coatings were evaluated for their cytocompatibility using human bone-marrow derived mesenchymal stromal cells (BMSCs), *Staphylococcus epidermidis* (SE) biofilm formation and impact on the macrophage immune response against bacterial colonization. The aim of this study was to directly compare BG and HA coatings with regard to their ability to combine cytocompatibility, anti-biofilm activity and modulation of antibacterial immune responses, and to assess whether BG coatings provide a multifunctional advantage over conventional HA coatings for potential application in revision arthroplasty.

2. Materials and methods

2.1. Coating of Ti-6Al-4V alloy discs with 45S5-BG and HA

Commercially available 45S5-BG powder (Vitryxx MD01) was purchased from Schott (Mainz, Germany). Two powders with different particle sizes were considered, i.e., d_{90} and d_{10} values for K2: 16 +/− 4 μm and K1: 30 +/− 4 μm (manufacturer information). Test runs for APS indicated that K2 was not flowable, whereas K1 was sufficiently flowable for APS. However, it turned out that the particle size distributions specified by the manufacturer were inconsistent. Own investigations showed that the powder specified by K1 exhibited a different size distribution of 62 +/− 6 μm. The used hydroxyapatite powder was delivered by Oerlikon and had a particle size of 57 +/− 15 μm.

As substrate material Ti-6Al-4V alloy discs with a diameter of 15 mm (surface area: 176.7 mm^2) and a thickness of 3 mm were used. For BG, APS was applied using a current of 420 A, process gases of 46/4 slpm Ar/He and a stand-off distance of 200 mm. 14 spray passes resulted in a nominal coating thickness of about 200 μm. For HA, the process was run with a current of 450 A, 50 slpm Ar as process gas and a stand-off distance of 125 mm. Here, for 12 spray passes slightly higher coating thicknesses of about 270 μm resulted.

2.2. Characterization of microstructure, surface morphology and crystallinity

Crystallinity of the BG samples was tested using X-ray diffraction (XRD) analysis by means of a 4-circle-X-ray diffractometer type Seifert PTS, Ahrensburg, Germany and Fe-filtered Cokα – radiation. As primary aperture a pin hole collimator with a nominal diameter of ø 1 mm was used. On the secondary side a slit with an opening of 0.8° was applied in front of the scintillation counter. Diffractograms in the 2θ-range between 20 and 150° were recorded with a step size of $\Delta 2\theta = 0.025°$. XRD analyses were carried out at the as-sprayed surface and after careful layer removal by mechanical polishing at a depth of 100 μm. In addition to XRD analysis, cross sections were taken and materialographically prepared to resolve the microstructure of both coating materials by means of light optical microscopy (LOM) and scanning electron microscopy (SEM). The SEM images are taken using SEM type Zeiss LEO 1530, Oberkochem, Germany and a backscattered electron detector at an acceleration voltage of 1 kV and a working distance WD of 6.5 mm. Three-dimensional topography was qualitatively assessed using a digital microscope (VHX-5000; Keyence Deutschland GmbH, Neu-Isenburg, Germany) with color-coded height mapping to visualize surface elevations and depressions. Surface roughness of the coatings was measured using a tactile stylus profilometry method with an Mahr M2 measurement system (Göttingen, Germany). Roughness parameters Ra and Rz were evaluated from the roughness profile (R-profile) after filtering with a robust Gaussian filter according to ISO 13565 using a cut-off wavelength of $\lambda c = 0.80$ mm. Instrumented indentation testing was carried out according to DIN ISO 14577 using microhardness testing system type Fischerscope HM100 (Fischer, Sindelfingen, Germany) using a maximum test load of 1 kN and a Vickers pyramid as indenter.

2.3. BMSC isolation

BMSCs were obtained from the bone marrow of patients undergoing elective hip replacement surgery. Cells were cultivated in cell culture flasks (Sarstedt, Nümbrecht, Germany) coated with 0.1% gelatin (Sigma Aldrich, Steinheim, Germany) using expansion medium (EM), consisting of Dulbecco's modified Eagle's medium (DMEM) high glucose, 12.5% fetal calf serum (FCS), 2 mM L-glutamine, 1% non-essential amino acids (NEAA), 50 μM β-mercaptoethanol (all Thermo Fisher Scientific, Dreieich, Germany), 100 μg/ml penicillin/streptomycin (Sigma-Aldrich) and 4 ng/ml fibroblast growth factor 2 (Active Bioscience, Hamburg, Germany) under standard cell culture conditions (37 °C and 5% CO_2 in a humidified atmosphere). Twenty-four hours after isolation medium was exchanged to discard non-adherent cells and thereafter three times per week. BMSCs of 10 donors were pooled to compensate inter-individual variations in cell behavior as described previously [28]. Cells were passaged at 80% confluency and stored in liquid nitrogen until further use. For the experiments, BMSCs in passage 5 were used.

Before bone marrow collection written consent from all patients was obtained. Harvesting and utilization of BMSCs were approved by the responsible ethics committee of the Medical Faculty of the University of Heidelberg (S-340/2018).

2.4. Seeding of surfaces with BMSCs, determination of cell viability and number

For cell culture experiments, non-coated or BG or HA coated Ti-6AI-4 V discs were sterilized at 160 °C for 30 min. The discs were pre-treated with DMEM, 10% FCS and 100 μg/ml penicillin/streptomycin (cultivation medium, CM) for 24 h at 37 °C and 5% CO_2. Thereafter, 6×10^4 BMSCs were seeded on each disc and further cultivation was performed in a 12 well plate in CM. BMSCs seeded in the same density on cell culture plastic (CCP) served as controls. After 72 h, BMSC viability was documented using fluorescein diacetate (FDA; Sigma Aldrich) staining. After a washing step with Dulbecco's Phosphate Buffered Saline (DPBS; Thermo Fisher Scientific), the discs were incubated with 6 μM FDA in DPBS for 2 min at 37 °C and rinsed with DPBS. Immediately thereafter, images were obtained from each disc with a fluorescence microscope (BZ-X810; Keyence Deutschland GmbH, Neu-Isenburg, Germany). Nuclear staining was performed with 4′,6-diamidino-2-phenylindole (DAPI; Thermo Fisher) for determination of the cell number. BMSCs were fixated with RotiHistofix (Carl Roth, Karlsruhe, Germany) for 20 min at room temperature followed by three times washing with DPBS. After permeabilization with 0.05% Tween 20 (Sigma Aldrich) in DPBS for 5 min and three washing steps with DPBS, nuclei were stained with DAPI (1 μg/ml in DPBS) for 5 min. Shortly after staining, four images were obtained from each sample with a fluorescence microscope (BZ-X810;). Cell nuclei were counted with the CellProfiler software [29] and used to calculate the mean count of cells per area.

2.5. In vitro biofilm formation and preparation of biofilm culture supernatants

Staphylococcus epidermidis (SE) strain RP62A (DSM 28319), a well-known in vitro biofilm producer [30] was used in this study. Bacteria were cultured on Columbia agar plates with 5% sheep blood (BD, Heidelberg, Germany) and streaked onto fresh agar plates a day before set-up of experiment. On the day of experiment, 3 to 5 colonies were transferred into trypticase soy bouillon (TSB; BD) and cultivated under shaking for 3 h at 37 °C to receive growth state bacteria. Bacterial density was measured photometrically (Den-1, Grant Instruments Ltd, Cambridge, UK) and adjusted to a concentration of $6*10^5$ CFU/ml in DMEM high glucose (Anprotec, Bruckberg, Germany) supplemented with 10% heat-inactivated fetal calf serum (FCS; Biochrom GmbH, Berlin, Germany). The respective Ti-6Al-4V discs were placed in a 12 well plate and 2 ml of bacteria suspension were added in each well. For the cell culture plastic control (CCP), respective bacteria amounts were plated in empty wells. Plates were incubated under static conditions for 3 days at 37 °C and 5% CO_2 with a careful medium exchange every 24 h. Day 1 and day 3 media of the biofilm cultures were collected and centrifuged at 4000 rpm for 15 min at 4 °C. Supernatants were then sterile filtered through a 0.2 μm filter and stored at −70 °C.

2.6. Crystal violet staining

Wells were carefully washed three times with ddH_2O to remove non-adherent bacteria. Biofilm matrix was stained with 0.1% Crystal Violet (Sigma-Aldrich, Taufkirchen, Germany, solved in ddH_2O) for 10 min at RT. After removing the staining solution, wells again were carefully washed three times with ddH_2O to remove non-bound dye. Wells were dried overnight with lid open under a fume hood. Matrix-bound dye was resolved by adding 30% acetic acid solution (Sigma-Aldrich) to each well for 10 min at RT. Supernatant was transferred into a 96 well plate and absorbance was measured at 540 nm using a CLARIOstar® Plus microplate reader (BMG Labtech, Ortenberg, Germany).

2.7. Lactate detection

Lactate concentration was measured using an enzyme-based bioluminescent assay according to the manufacturer's protocol (Lactate-Glo™ Assay, Promega GmbH, Walldorf, Germany). Supernatants were diluted 1:500 with PBS, a standard curve with defined L-lactate concentrations (0–200 μM) was included. Samples and standard were incubated with the lactate detection reagent for 1 h at RT and light emission was recorded using a CLARIOstar® Plus microplate reader (BMG Labtech, Ortenberg, Germany).

2.8. Stimulation of macrophages

The murine macrophage cell line RAW 264.7 (ATCC TIB-71, USA) was cultivated in DMEM high glucose supplemented with 10% heat-inactivated FCS and 1% Penicillin/Streptomycin at 37 °C and 5% CO_2. For experiments, cells were transferred into suitable well plate formats and stimulated with biofilm supernatants 1 to 4 diluted in fresh culture media. Cell numbers and time points were used as follows: for gene expression analysis, 0.5 million cells/ml were added into a 48 well plate and stimulated for 8 h; 2 million cells/ml were added into a 12 well plate and stimulated for 4 h for immunoblotting of NF-κB pathway activation. For the other read-outs, 2 million cells were transferred into 6 well plates and stimulated for 20 h in a total volume of 2 ml. Supernatants were collected and used for detection of lactate and cytokine release. 0.5 million cells were used for phagocytosis assay or MHC II and CD86 surface marker staining, respectively. 1 million cells were used for immunoblotting of STAT1 and STAT3 pathway activation.

2.9. Gene expression analysis

Total RNA was extracted using the innuPREP RNA Mini Kit 2.0 (AJ Innuscreen GmbH, Berlin, Germany) according to the manufacturer's protocol. 1 μg of total RNA were transcribed into cDNA using the RevertUPTM II cDNA synthesis Kit (biotechrabbit GmbH, Hennigsdorf, Germany) according to the manufacturer's protocol with a combination of oligo (dT) and hexamer primers. A noRT sample (without Reverse Transcriptase) was included. Two microliters of a 1:1 diluted cDNA template were transferred into a two-step PCR reaction (StepOnePlus Real-Time PCR Cycler, Applied Biosystems, Darmstadt, Germany) using the 2× qPCRBIO SyGreen Mix Hi-ROX (PCR Biosystems Ltd., London, UK). Specificity of PCR products were controlled by melting curve comparison with noRT and water samples. The reference gene *Hprt1* was used for normalization and mRNA levels of the genes of interest were calculated by the $2^{-\Delta Cq}$ method. Primer sequences are listed in Table 1.

Mouse specific primers were designed intron-flanking and included all transcript variants if possible and were obtained from *biomers.net* GmbH (Ulm, Germany). If more transcript variants are present, RefSeq is given for transcript variant 1.

2.10. Phagocytosis assay

Cells in media were transferred into Eppendorf reaction tubes, 10 μl fluorescence-labeled latex beads (Sigma-Aldrich, Taufkirchen, Germany, 1 to 10 diluted in PBS) were added, mixed and incubated for 30 min at 37 °C and 5% CO_2. Cells were washed twice with cold PBS, resuspended in cold PBS and kept on ice until analysis. Bead uptake per cell was measured with the BD FACSCanto™ Flow Cytometer (BD Biosciences, Heidelberg, Germany) and analyzed using the BD FACS Diva software (version 5.0.3).

2.11. FACS

After washing twice with PBS, cells were resuspended in 100 μl PBS/

Table 1
List of oligonucleotides used for quantitative RT-PCR analysis.

Gene	RefSeq	Forward primer	Reverse primer
Arg1	NM_007482.3	TCACCTGAGCTTTGATGTCG	CACCTCCTCTGCTGTCTTCC
Hprt1	NM_013556.2	GGGGACATAAAAGTTATTGGTGG	CATTTTGGGGCTGTACTGCT
Ifnb	NM_010510.1	TGGGAGATGTCCTCAACTGC	CCAGGCGTAGCTGTTGTACT
Il6	NM_031168.2	CCGGAGAGGAGACTTCACAG	TTCTGCAAGTGCATCATCGT
Il10	NM_010548.2	GGTTGCCAAGCCTTATCGGA	ACCTGCTCCACTGCCTTGCT
Irg1	NM_008392.1	CAGCTCTATCGGAAGCCCTG	CAGAAACTTGGACGCAGCAG
Nos2	NM_010927.4	CATGAGCTTGGTGTTTGGGTG	TCCGCAAATGTAGAGGTGGC
Tnfa	NM_013693.3	AAAATTCGAGTGACAAGCCTGTAG	CCCTTGAAGAGAACCTGGGAGTAG

2% BSA and 0.2 mg/ml of PE anti-MHC II (Invitrogen, (Thermo Fisher Scientific), Dreieich, Germany) and APC anti-CD86 (BioLegend, San Diego, CA, USA) antibodies were added for 1 h at 4 °C. Cells were washed two times with PBS, resuspended in 300 µl PBS and analyzed with the BD FACSCanto™ Flow Cytometer. Results were further analyzed using the BD FACS Diva software (version 5.0.3).

2.12. Immunoblotting

Protein isolation was performed in RIPA lysis buffer (1% *v*/v NP-40 (IGEPAL® CA-630), 0.25% sodium deoxycholate, 50 mM Tris pH 8.0, 150 mM NaCl, 1 mM EDTA pH 8.0, 1 mM Na3VO4) containing protease inhibitors (Protease Inhibitor Mix G) and phosphatase inhibitors (Phosphatase Inhibitor Mix II, both Serva Electrophoresis GmbH, Heidelberg, Germany) for 1 h at 4 °C. 10 µg protein were separated at 120 V using pre-cast gradient 4–20% Tris-glycine gels (anamed Elektrophorese GmbH, Rodau, Germany). Proteins were transferred onto an AmershamTM ProtranTM 0.45 µm nitrocellulose membrane (GE Healthcare, Chicago, IL, USA) in transfer buffer (192 mM glycine, 25 mM Tris, 2.6 mM SDS, 0.5 mM Na_3VO_4, 15% v/v methanol) for 1 h at 2 mA/cm^2. Blocking occurred in BlueBlock PF (Serva Electrophoresis GmbH) with 0.5 mM Na_3VO_4 for 30 min at RT, membranes then were incubated with primary antibodies (listed in Table 2) in BlueBlock PF + Na_3VO_4 either over night at 4 °C or 4 h at RT. Protein visualization was done after incubation with the respective HRP-linked secondary antibody (1:1000, HRP-linked goat anti-rabbit IgG, Cell Signaling Technology, Danvers, MA, USA) for 1 h at RT using ECL substrate (WESTAR ETA C ULTRA 2.0, Cyanagen Srl, Bologna, Italy) and a ChemoStar ECL and Fluorescence Imager (Intas Science Imaging Instruments GmbH, Göttingen, Germany).

Antibodies were all recommended for use in mouse and applied according to the manufacturer's advice. Proteins were detected by chemiluminescent luminol reaction after incubation with respective HRP-linked secondary antibody and imaged in a ChemoStar ECL Imager (Intas Science Imaging Instruments GmbH).

2.13. Cytometric bead array (CBA)

CBA (LEGENDplex™, BioLegend, San Diego, CA, USA) was performed according to the manufacturer's protocol. A Mouse Inflammation Panel (Mix and Match Subpanel) including TNF-α, IL-10, IFN-β and IL-6 beads was used. Centrifuged supernatants were diluted 1:5 with Assay Buffer and transferred into a V-bottom plate. A standard was included. After addition of the bead mix to the samples, the plate was incubated over night at 4°C in the dark while shaking. After washing, samples were incubated with the detection antibody for 1 h at RT, streptavidin-phycoerythrin (SA-PE) was added and the mixture was further incubated for 30 min at RT with shaking. Samples were analyzed using the MACSQuant 10 (Miltenyi Biotec B.V. & Co. KG, Bergisch Gladbach, Germany), and cytokine concentrations were calculated with the LEGENDplex™ Data Analysis Software (https://legendplex.qognit.com).

Table 2
List of antibodies used for Immunoblotting (Western Blot).

Protein	Source	Size (kDa)	Dilution	Company
β-Actin	Rabbit	42	1:1000	Proteintech, USA
Phospho-NFκB p65 (Ser536)	Rabbit	65	1:1000	Cell Signaling Technology, USA
Phospho-STAT1 (Tyr701)	Rabbit	84, 91	1:1000	Cell Signaling Technology, USA
Phospho-STAT3 (Tyr705)	Rabbit	79, 86	1:1000	Cell Signaling Technology, USA

2.14. Statistical analyses

All experiments were performed in three independent replicates ($n = 3$), each using separately prepared coated Ti-6Al-4V discs (non-coated, Ti; hydroxyapatite coated, HA; or 45S5-BG coated, BG) and cell culture plastic (CCP), respectively. Due to the multi-step experimental setup, including coating preparation, biofilm formation and subsequent macrophage stimulation with collected supernatants, a certain degree of variability between replicates is expected. Mean ± standard deviation is shown with single values presented as dots. For statistical evaluation, an ordinary one-way analysis of variance (ANOVA) including post-hoc multiple comparison testing and Bonferroni correction was performed. A p-value <0.05 was considered statistically significant. Statistical analysis was done with GraphPad Prism for Windows (version 9.3.1; GraphPad Software Inc., San Diego, CA, USA).

3. Results

3.1. Microstructure, surface morphology and crystallinity

X-ray diffraction analysis on the coated BG samples revealed that the glass coating was entirely amorphous. No diffraction lines from crystalline fractions could be resolved (Suppl. Fig. 1, a1 and a2).

Surface roughness was characterized by the arithmetical mean roughness (Ra, center line average) and the mean peak-to-valley height (Rz). Analysis of surface topography revealed that HA coated samples exhibited a lower surface roughness, with an Ra of 6.69 ± 0.56 µm and an Rz of 34.80 ± 3.26 µm, compared to BG-coated samples, which showed an Ra of 10.25 ± 0.99 µm and an Rz of 51.14 ± 4.89 µm (Fig. 1, a1 and a2). These differences in surface morphology were further confirmed by three-dimensional surface mapping, demonstrating the increased roughness of the BG coating relative to HA (Fig. 1, b1 and b2).

The SEM-BSD images indicate typical structures for thermally sprayed coatings of BG and HA where the deformed splats of individually particles can be resolved. While the HA coating is rather compact with no visible pores, the BG coating indicates a rather large porosity (Fig. 2, a1 and a2). Using three SEM images with the resolution shown in Fig. 2a2, a porosity of about 9.72% ± 1.54% was calculated for the BG coating in average using the image processing software ImageJ, while single pores can reach sizes of about 20–30 µm. Top-view SEM images of the BG surface revealed predominantly rounded splats without sharp features, which is characteristic of APS coatings. In addition, partially unbonded particles were observed (Fig. 2, b1 and b2). Qualitative assessment showed that both coatings were continuous and free of

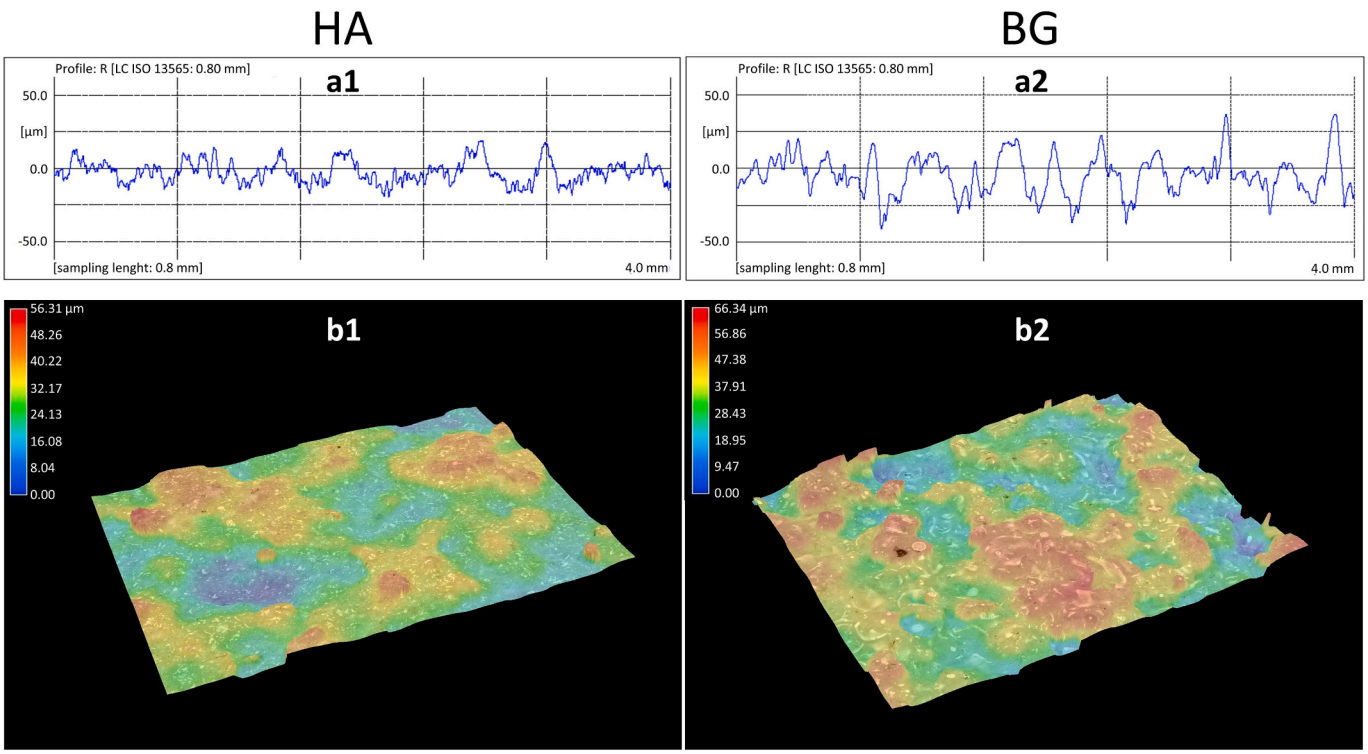

Fig. 1. Morphological analysis of the coatings. (a) HA coating and (b) BG coating. (a1) and (b1) show the roughness of the HA and BG coating, respectively. (a2) and (b2) shows their three-dimensional surface topography.

chipping. Cross-sectional metallographic analysis further revealed a homogeneous and well-bonded interface between the coating and the substrate, without visible cracks or delamination, indicating strong adhesion (Suppl. Fig. 1, b1 and b2). This is consistent with the residual stress measurements, which showed smooth and continuous strain relaxation behavior without any kinks (Suppl. Fig. 1, c1 and c2) indicating the absence of interfacial failure during drilling and indirectly confirming good coating adhesion.

Instrumented hardness testing according to DIN ISO 14577 using a load of 1 kN and a Vickers pyramid indenter revealed the characteristic values of Martens hardness (HM), indentation modulus (E_{IT}) and the plastic part of the indentation work (η_{plast}) for both coatings as listed in Table 3.

3.2. Cytocompatibility of the coatings and BMSC number

FDA staining revealed viable cells in all groups (Fig. 3a). When qualitatively compared to CCP, the cytoplasm of the BMSCs seeded on the coated surfaces appeared to be smaller and the cell bodies were stretched while the number and distribution of the nuclei was comparable (Fig. 3a). Furthermore, the cell layer on the Ti-6AI-4V surface appeared dense and ordered, following possible smaller, circular scratches on the Ti-6AI-4V surface that are most likely a result of cutting the Ti-6AI-4V discs from a rod. Cells grown on Ti-6AI-4V and CCP showed increased viability compared to cells grown on the HA and BG coated surfaces, respectively (Fig. 3b). No differences in cell viability between HA and BG coating were detectable. However, the number of cells did not differ between the groups: while there was a relative maximum detectable in in the Ti-6AI-4V group, no significant differences were detected (Fig. 3c). Thus, both surface coatings show a comparable cytocompatibility.

3.3. BG coating significantly reduced SE biofilm formation compared to HA

Biofilm formation of the used SE strain significantly increased on non-coated Ti-6Al-4V discs (Ø 10 mm) over time and showed a strong matrix deposition after 3 days according to CV staining (Fig. 4a+b). Thus, day 3 was used for following evaluation of biofilm formation on the different coatings (Fig. 4c-e). As shown in Fig. 4d, remarkable differences were observed between the differently coated Ti-6Al-4V discs with reduced media acidification as indicated by a less pronounced color change toward yellow of the phenol red pH indicator and deposition of a slimy biofilm matrix by BG. CV staining further showed that HA exhibited the highest and BG the lowest biofilm mass (Fig. 4c). pH measurements of day 2 supernatants further confirmed a higher pH in the BG group (Table 4). Interestingly, the reduced decrease in pH in the BG group was not due to reduced lactate release by the smaller biofilm as lactate concentration was even lower in the HA group (Fig. 3e). Suppl. Fig. 2a shows background staining (for all, OD at 540 nm < 0.2) and basal lactate levels (for all, ca. 2 mM) of the samples cultured without SE.

pH values were measurement using indicator strips as shown in Suppl. Fig. 3. Table shows the range of pH of $n = 5$ for CCP or $n = 3$ for Ti, HA and BG, respectively. pH of respective samples cultured without SE is stated in brackets.

3.4. BG coating allows for immunocompetence against colonization with SE

Day 1 media of the SE biofilm cultures on the different Ti-6Al-4V discs were collected and effects of coatings on macrophage immune activation against bacterial colonization was analyzed. All supernatants induced expression of *Nos2*, the gene encoding for the inducible nitric oxide synthase (iNOS) generally used as marker for proinflammatory M1 macrophage polarization. Arginase 1 (Arg1) gene expression is associated with a more anti-inflammatory M2 macrophage polarization [31].

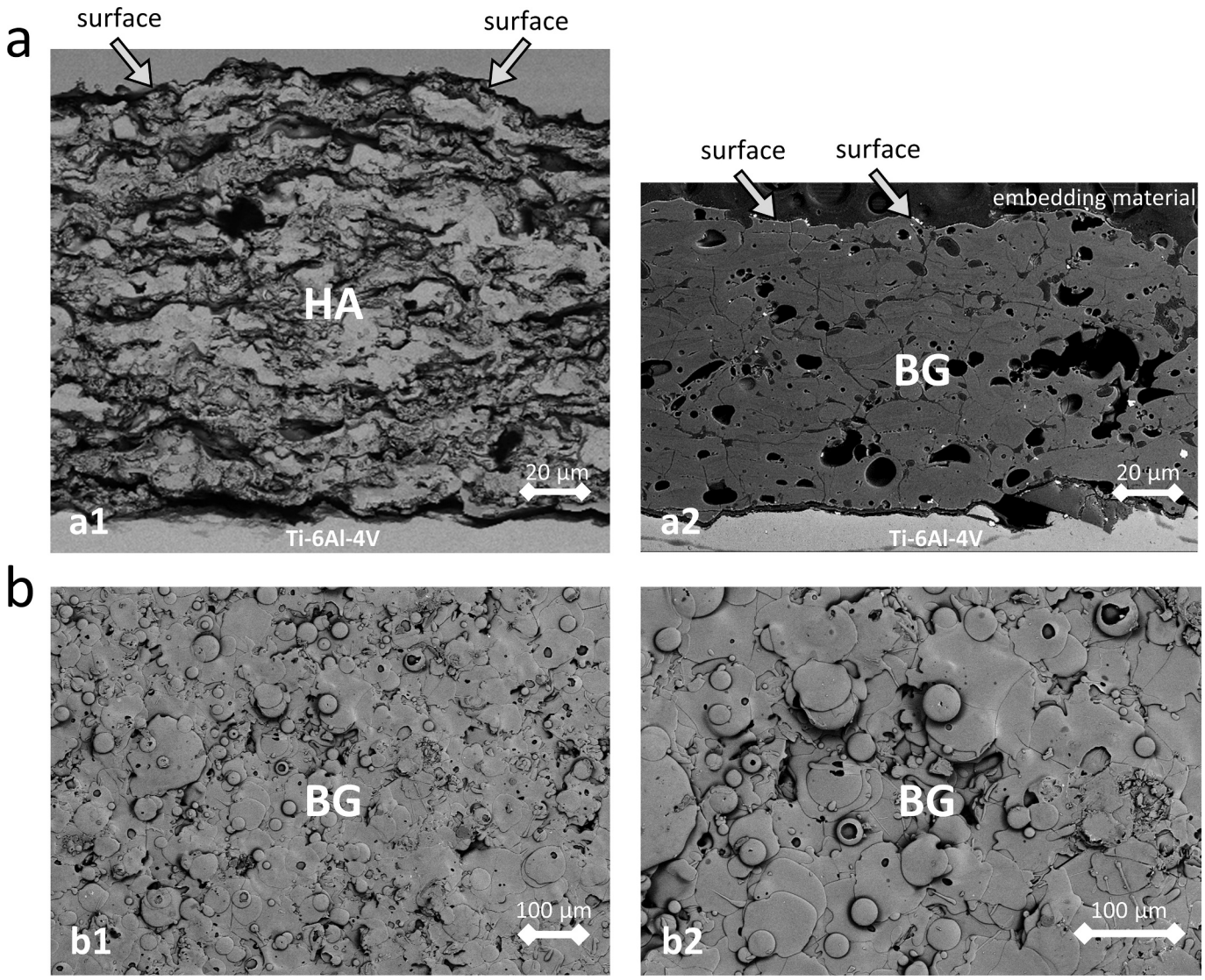

Fig. 2. Scanning electron microscopy (SEM) analysis of the coatings. (a) Cross-sectional SEM images (BSE contrast – 300× magnification) of HA coating (a1) and BG coating (a2). The microstructure of the coatings with interface to the Ti-6Al-4V disc is shown. (b) SEM images (BSE contrast, left: 100 x and right 200 x magnification) showing the surface of the BG coating.

Table 3
Characteristic values from instrumented indentation according to DIN ISO 14577, average values for 20 indentations for each coating.

	HM [MPa]	E_{IT} [GPa]	η_{plast} [%]
HA	1584 ± 345	51 ± 12	77 ± 4
BG	2220 ± 587	55 ± 10	62 ± 5

Interestingly, BG coating further increased *Nos2* whilst reducing *Arg1* expression indicating a more pro-inflammatory macrophage phenotype (Fig. 5a) which resulted in an overall more M1 polarized macrophage phenotype in the BG group (Fig. 5b). Immune regulatory gene 1 (*Irg1*) encodes for the aconitate decarboxylase 1 (ACOD1), a key regulator of immunometabolism that induces breaks in the tricarboxylic acid (TCA) cycle and promotes a metabolic shift toward glycolysis, thereby serving as an indicator of an inflammatory response [32]. *Irg1* mRNA levels are highly up-regulated upon stimulation with all biofilm supernatants in line with increased glycolytic lactate production (Fig. 5c+d). Furthermore, increased NF-κB signaling indicated a strong toll-like receptor (TLR) activation by all supernatants. Early activation of the STAT3 pathway, however, most likely was related to the high levels of biofilm-derived lactate in the supernatants (Fig. 5e). Phagocytotic activity as well as major histocompatibility complex II (MHC II) and co-stimulatory molecule CD86 both related to antigen presentation were up-regulated upon stimulation with the biofilm supernatants and were highest in the HA group (Fig. 5f+g). There is no immune activation detectable upon stimulation with the supernatants of the respective samples without SE (Suppl. Fig. 1b-f).

We further investigated cytokine production by the macrophages upon stimulation with media of day 1 SE biofilm cultures on the differently coated Ti-6Al-4V discs (Fig. 6). While so, we found TNF-α and IL-10 being up-regulated by all supernatants compared to the unstimulated control. TNF-α release was most pronounced in both, the HA and BG coating group, whereas IL-10 concentration was highest in the HA group (Fig. 6a+b). Ultimately, this leads to a pro-inflammatory M1 macrophage polarization which was slightly increased in the BG group compared to HA (Fig. 6c). Like TNF-α and IL-10, also the cytokines IL-6 and IFN-β were induced by all SE biofilm supernatants (Fig. 6d+e). Interestingly, for both cytokines, concentrations were highest in the HA group whereas BG showed similar results than non-coated Ti-6Al-4V discs or cell culture plastic (Fig. 6e). In line with this, subsequent STAT signaling was activated by all supernatants with strongest activation

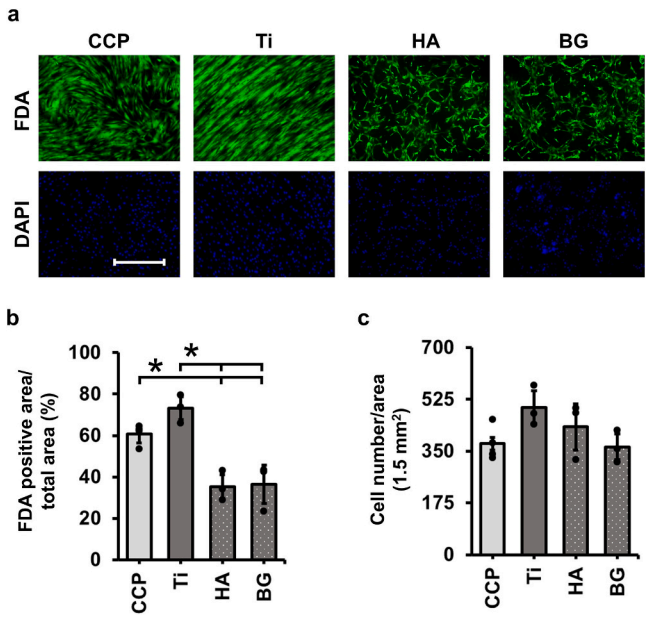

Fig. 3. BMSC viability, morphology and number on the different surfaces. (a) Fluorescence microscopy shows viable cells and comparable growth patterns for the coatings. (b) Shows the relative viability in a defined area of 1.5 mm^2. Significant differences between the groups as shown by the brackets are highlighted by (*). (c) Shows the cell number in a defined area of 1.5 mm^2, no significant differences were detectable.

again detected in the HA group (Fig. 6f). The strong macrophage activation observed in the HA group appeared to correlate with the higher biofilm mass and therefore was most likely related to the increased bacterial load. No differences were seen for TNF-α, IL-6 or IFN-β upon stimulation with supernatants cultivated with the differently coated Ti-6Al-4V discs or CCP without SE (Suppl. Fig. 1g-i). However, an increase in IL-10 concentration could be detected for all Ti-6Al-4V discs (Ti, HA and BG) with highest amount found for BG (Suppl. Fig. 1g).

In order to evaluate the impact of the differently coated Ti-6Al-4V discs on immune activation against formed SE biofilms, we further investigated macrophage gene expression upon stimulation with supernatants of day 3 SE biofilm cultivated on the different surfaces (Fig. 7). Expression of *Nos2* was still highest and *Arg1* lowest induced by the environment of biofilms grown on BG (Fig. 7a), maintaining a more pronounced M1 polarization in the BG group (Fig. 7b). mRNA levels of the cytokines *Tnfa*, *Il10*, *Il6* and *Ifnb* equalized between the different groups (Fig. 7b+c).

4. Discussion

One of the most common cause of failure for revision arthroplasty is infection – when infection was the reason for revision surgery of hip joints, the 5-years survival rate was with 67% significantly worse when compared to a 5-years success rate of 84.4% in patients with aseptic loosening as reason for revision [4]. To overcome this, the functionalization of implant surfaces that addresses both, improved osseointegration and antibacterial activity, are under current investigation. 45S5-BG is well known for its osteoconductive properties and frequently used as a bone graft material in orthopedic surgeries with promising results [13,14]. Furthermore, 45S5-BG was shown to assess antimicrobial

Table 4
pH values of the supernatants at day 2 of SE biofilm cultivation on the different coatings.

	CCP (n = 5)	Ti (n = 3)	HA (n = 3)	BG (n = 3)
pH	5.0–5.3 (8.7)	5.3–5.8 (8.7)	5.5–6.1 (8.7)	8.1–8.5 (9.0)

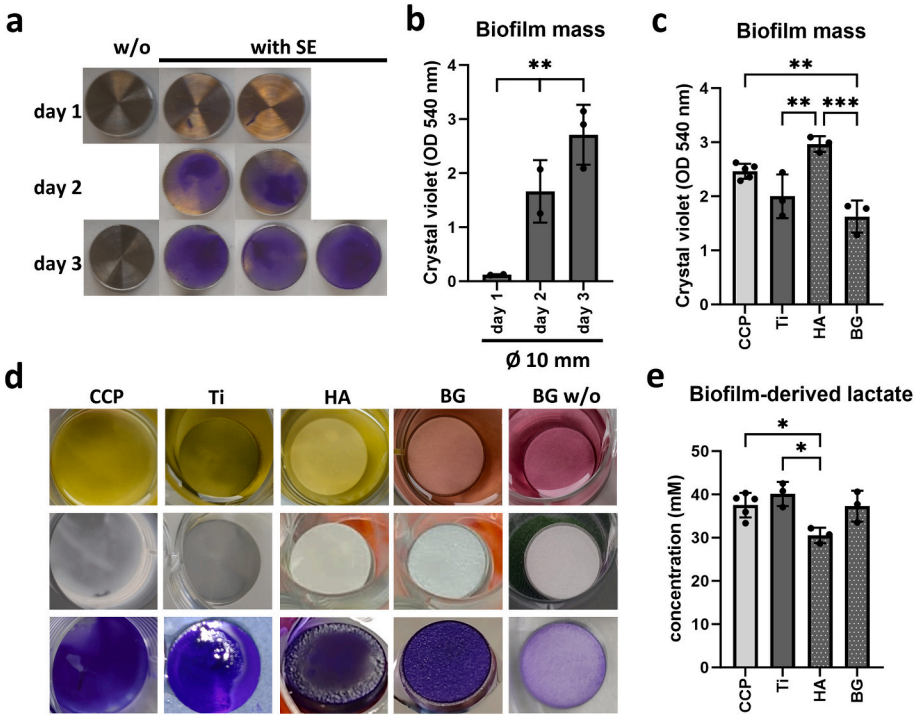

Fig. 4. Impact of HA and BG coatings on SE biofilm formation. Biofilm formation of SE strain RP62A on CCP, non-coated, HA or BG coated Ti-6Al-4V discs. (a + b) Validation of biofilm formation on Ti-6Al-4V discs (diameter: 10 mm) at day 1, 2 and 3 by CV staining (a) and quantification (b). (c) CV quantification of biofilms formed after 3 days, corrected for background staining of samples without SE. (d) Representative images of biofilm formation at day 3: top panels show samples shortly before collecting the supernatants, middle panels show samples prior to CV staining, and bottom panels show samples immediately after CV staining. (e) Lactate release by day 3 biofilms, corrected for baseline lactate levels of samples without SE.

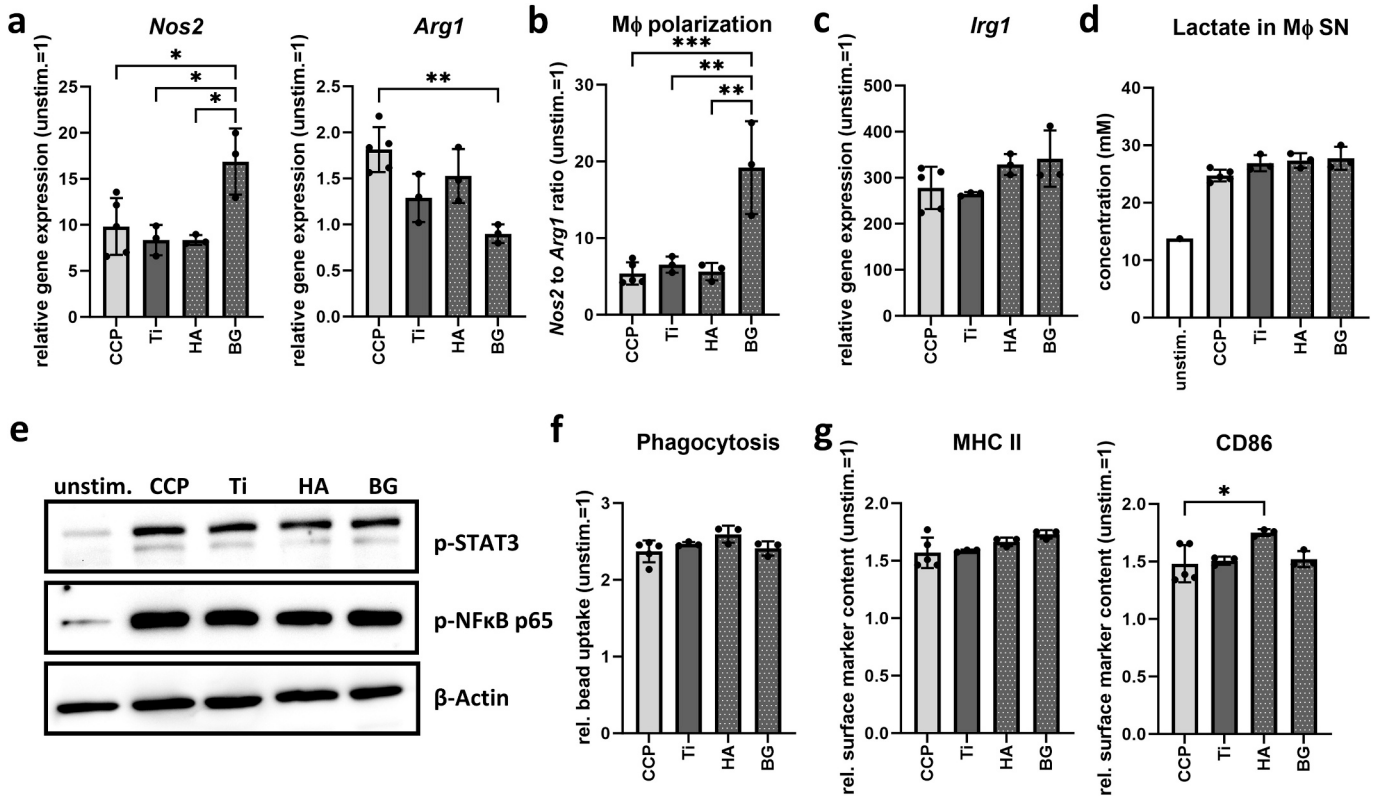

Fig. 5. Impact of HA and BG coatings on macrophage activation by bacterial colonization. RAW 264.7 macrophages were stimulated with day 1 supernatants from SE biofilms grown on non-coated, HA or BG coated Ti-6Al-4V discs. (a–c) Gene expression of M1 marker Nos2, M2 marker Arg1, and immunometabolism regulator Irg1 after 8 h, normalized to the reference gene Hprt1 and the unstimulated control; (b) Nos2/Arg1 ratio as indicator of macrophage polarization. (d) Lactate levels in macrophage supernatants after 20 h. (e) Activation of NF-κB and STAT3 signaling after 4 h (Western blot; β-actin as loading control). (f, g) Phagocytotic activity and surface expression of MHC II and CD86 after 20 h, normalized to the unstimulated control.

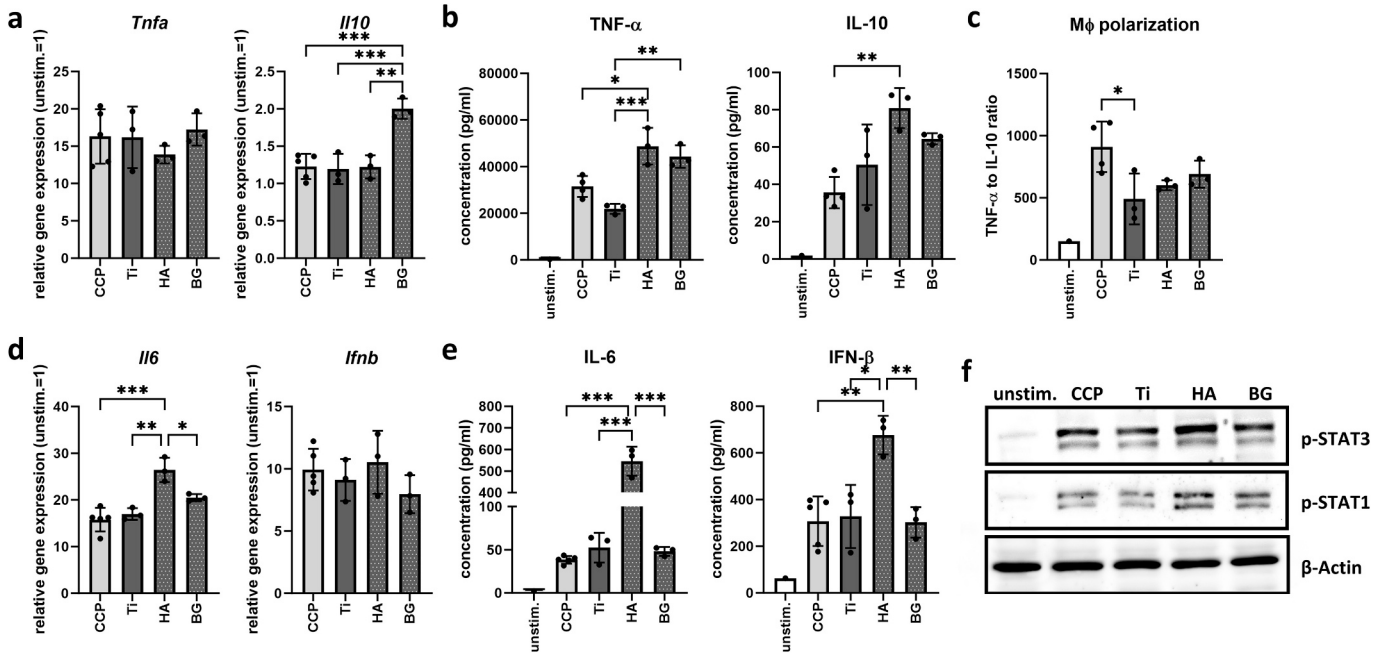

Fig. 6. Impact of HA and BG coatings on macrophage cytokine response to bacterial colonization. RAW 264.7 macrophages were stimulated with day 1 supernatants from SE biofilms grown on non-coated, HA or BG coated Ti-6Al-4V discs. (a, d) Gene expression of pro- and anti-inflammatory cytokines (Tnfa, Il10, Il6, Ifnb) after 8 h, normalized to the reference gene Hprt1 and the unstimulated control. (b, e) Cytokine release (TNF-α, IL-10, IL-6, IFN-β) in macrophage supernatants after 20 h quantified by LEGENDplex™. (c) Macrophage polarization indicated by TNF-α/IL-10 ratio. (f) Activation of STAT1 and STAT3 signaling after 20 h (Western blot; β-actin as loading control).

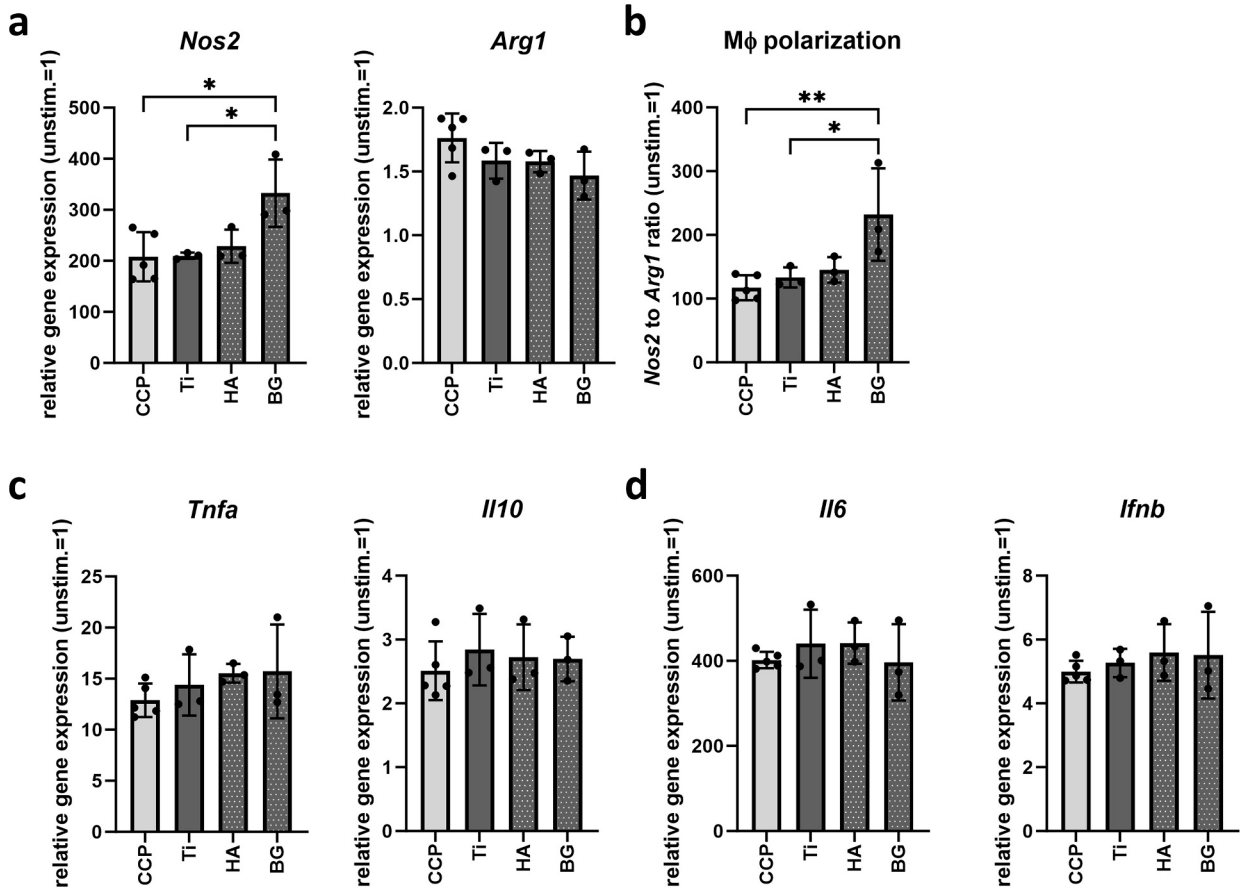

Fig. 7. Impact of HA and BG coatings on macrophage immune response to SE biofilms. RAW 264.7 macrophages were stimulated with day 3 supernatants from SE biofilms grown on non-coated, HA or BG coated Ti-6Al-4V discs. (a-d) Gene expression of M1 marker Nos2, M2 marker Arg1, and cytokines (Tnfa, Il10, Il6, Ifnb) after 8 h, normalized to the reference gene Hprt1 and the unstimulated control; (b) Nos2/Arg1 ratio as indicator of macrophage polarization.

activity against a broad range of bacteria strains including staphylococci species [33,34]. However, most studies to date have used bioactive glass in particulate form, comparing the effects of particle size or different glass compositions on biological outcomes. In this study, we employed an APS process, which allowed the fabrication of clinically applicable 45S5-BG coating and a direct comparison with state-of-the-art HA coating. Through APS, the powdered material is injected into the plasma jet at high speed, while the extreme heat melts the particles as they move toward the substrate. Once they reach the surface, the molten particles instantly flatten and solidify, forming thin layers known as splats. By this, APS results in rather dense coatings with a strong mechanical bond between the coating and the substrate, promoting adhesion [35]. The metallographic investigations of our samples suggest that both coating systems (HA and BG) exhibit good adhesion to the substrate. The microstructures deposited within the project are typical for thermally sprayed HA coatings. The SEM images show the characteristic splat structure that forms during deposition and the HA layers can be described as having an almost pore-free structure. When selecting the coating parameters, it is important to ensure that the BG does not crystallize, as this would negatively affect its bioactive properties. This could be ruled out in the study presented here; XRD revealed that the layers are amorphous. However, with the process parameters used, APS results in an average porosity of slightly less than 10%, with pore sizes that can individually reach 20–30 μm which is in the range reported by others [27,36]. In line with the study by Garrido et al. [36], roughness indicated by Ra and Rz was higher for 45S5-BG than HA coatings. Furthermore, the indentation-derived mechanical properties (HM, E_{IT} and η_{plast}) determined in this study fall within the expected range for plasma-sprayed HA and BG coatings.

We evaluated the effect of the BG coating on attachment and survival of BMSCs as well as SE biofilm formation and macrophage activation by bacterial colonization. To our knowledge, this is the first study investigating these critical aspects in direct comparison to HA coated Ti-6Al-4V alloys. Our data show that viability and numbers of attached BMSCs were the same between both coatings and thus were not negatively affected by the BG. Remarkably, biofilm formation was significantly reduced on BG coated Ti-6Al-4V discs compared to HA and CCP and still slightly less than plain Ti-6Al-4V. Furthermore, acidification of the environment by biofilm formation was less with BG coating, which was independent of biofilm derived lactate levels. In addition, we evaluated macrophage activation upon stimulation with the different SE biofilm supernatants and found that BG coating allowed for a strong pro-inflammatory M1 polarized macrophage immune response against bacterial colonization and biofilm formation. All required pathways for antigen presentation and subsequent T cell activation were similarly induced in the BG environment together with a robust production of infection-associated cytokines.

45S5-BG is well known to support the survival of MSCs from various sources and to promote their osteogenic differentiation capacity [37–40]. In line with these reports, we observed viable cells and sufficient cell numbers on the BG coated Ti-6Al-4V surfaces, comparable to the clinically established HA coating. Although cell density and apparent cell size were reduced compared to CCP and plain Ti-6Al-4V, this does not necessarily indicate impaired cytocompatibility but rather reflects the distinct surface properties of the coatings. In contrast to the flat control surfaces, BG and HA coatings exhibit pronounced micro- and nano-scale topography, which affects cell adhesion, spreading and cytoskeletal organization. Therefore, the altered BMSC

morphology and reduced spreading area likely result from topography-driven cell–material interactions and reflect a more in vivo–like cell shape typical of rough and microtextured implant surfaces [41,42]. Overall, our BG coating support host cell survival and induce morphology changes comparable to clinically established HA.

However, while HA is well established for its biocompatibility, it lacks intrinsic antibacterial functionality. This highlights the need for advanced implant surfaces that not only maintain favorable host cell interactions but also actively prevent bacterial colonization. In this context, a recent study has emphasized the development of a dual-functional implant surfaces that simultaneously promote osseointegration and inhibit bacterial colonization [43]. The BG coating investigated in the present study may provide a comparable dual functionality, linking favorable cell compatibility with antibacterial effects. Consistent with this concept, biofilm formation was significantly reduced on BG compared to HA, while host cell attachment was not impaired. Among all surfaces, the HA coating exhibited the highest biofilm biomass, consistent with a previous report demonstrating enhanced *Staphylococcus aureus* adhesion to HA coated relative to uncoated titanium implants [44]. The biofilm-suppressive properties of 45S5-BG and its derivative S53P4 have been described previously [33,45–47], and our data support these findings, with the BG coating showing the lowest biofilm formation. Notably, whereas prior studies predominantly investigated the effects of BG particles added to biofilms growing on different materials, our study assessed biofilm formation directly on the coated BG surface, which, to our knowledge, has not been reported before. In addition, biofilm formation was evaluated under physiologically relevant conditions containing cell culture medium supplemented with serum rather than bacterial broth. The mechanisms underlying the observed effects remain to be elucidated; however, local pH elevation and surface topography-mediated bacterial cell wall damage have been proposed as potential contributing factors [19,48]. As the BG splats exhibited a smooth and rounded morphology without sharp features, a mechanically induced bactericidal effect—such as membrane rupture caused by nanoscale surface protrusions (e.g., nanopillars on dragonfly wings [49])—appears unlikely. Despite the higher surface roughness of BG (Ra ≈ 10) compared to HA (Ra ≈ 7), bacterial attachment and biofilm formation were reduced on BG, indicating that roughness alone does not explain the observed differences. Both HA and BG are generally hydrophilic due to the presence of surface hydroxyl groups, and the higher roughness of BG may further enhance its hydrophilicity, consistent with the Wenzel model. As SE preferentially adheres to more hydrophobic surfaces via nonspecific physicochemical interactions [50,51], the hydrophilic character of BG may limit initial bacterial attachment. However, as experiments were performed in the presence of FCS, which forms a protein conditioning layer, the influence of intrinsic surface properties may be partially masked. Instead, the reduction in biofilm formation is more plausibly attributed to chemical effects. The initial release of alkaline ions from 45S5-bioactive glass, particularly Na^+, can lead to local alkalization via ion exchange processes [21]. Elevated pH levels are known to suppress bacterial adhesion and biofilm formation in both SE and the additionally clinically important pathogen *Staphylococcus aureus* [52]. Accordingly, the observed shift in pH from approximately 6 (HA) to 8.5 (BG) is likely to be a key factor contributing to the reduced biofilm formation.

However, such ion-mediated changes in the local microenvironment may not only affect bacterial viability but also influence host cell behavior and impact cellular responses. Recent studies suggest that careful tuning of ion release and pH levels is essential to balance host cell compatibility [53]. Beyond pH effects, specific ions have also been reported to actively regulate immune responses. For instance, metal ions such as Mn can modulate macrophage polarization and promote osteogenic processes by activating relevant signaling pathways [54], highlighting the broader role of ion-mediated immunomodulation in tissue regeneration and antibacterial defense. Bioactive glass has been reported to be less immunogenic under sterile, non-inflammatory conditions, which is consistent with our observations in bacterial-free control samples, while modulating macrophage activation upon inflammatory stimulation. In particular, exposure to 45S5-BG has been shown to reduce the production of the pro-inflammatory cytokines TNF-α and IL-6 while increasing anti-inflammatory IL-10 in human macrophages following LPS challenge [55]. In line with these findings, a recent study demonstrated that the 45S5-BG derivative S53P4 reverses the suppressive effect of LPS on oxidative phosphorylation in RAW 264.7 macrophages and promotes a more anti-inflammatory polarization, characterized by reduced *Il1b* and *Il6* expression, decreased IRF and NF-κB pathway activation, and diminished nitric oxide release [56]. Importantly, these effects were mainly mediated by changes in the extracellular environment rather than direct cell–material contact, indicating that ion release and pH modulation contribute to the immunomodulatory properties of bioactive glass. To exclude potential adverse effects of our BG coating on antibacterial macrophage activation, we examined the macrophage immune response induced by supernatants from SE biofilms formed on the respective coatings. For all samples we detected a pro-inflammatory macrophage signature upon stimulation with SE biofilm supernatants compared to non-stimulated control cells which is in line with data from a previous study [57]. Remarkably, supernatants derived from SE biofilms grown on BG coated surfaces induced a more pronounced M1-polarized macrophage phenotype, as indicated by increased *Nos2* and decreased *Arg1* expression levels together with elevated TNF-α production. From a functional perspective, M1-polarized macrophages are strongly associated with enhanced antibacterial activity, including the production of reactive oxygen and nitrogen species, pro-inflammatory cytokines and increased phagocytic capacity [58,59], all of which are critical for effective biofilm disruption and bacterial clearance. In contrast, M2 polarization has been linked to impaired bacterial clearance and biofilm persistence, as it is primarily associated with tissue remodeling and anti-inflammatory responses [60–62]. In this context, the activation of NF-κB and STAT signaling pathways plays a central role in regulating macrophage polarization and antibacterial immunity. NF-κB is a key driver of pro-inflammatory gene expression and M1 activation [63], while STAT3, acting as the principal effector of IL-10 signaling, counteracts NF-κB-driven inflammation and fine-tunes the balance between pro- and anti-inflammatory responses [64]. The enhanced M1 polarization observed in our study therefore suggests that BG-associated environmental changes support signaling pathways that favor antibacterial immune activation rather than suppressing it. In contrast to the previous reports describing suppressive effects of bioactive glass on macrophage pro-inflammatory activation following LPS stimulation, no attenuation of antibacterial immune activation was observed under biofilm-associated conditions in our study. These findings therefore suggest that BG coatings not only suppress biofilm formation directly but also preserve, and potentially support, host antibacterial immune responses, highlighting their promise for application in infection-prone revision arthroplasty.

A limitation of the present study is the use of the murine macrophage cell line RAW 264.7 to assess the effects of the coatings on antibacterial immune responses. While this model is widely used and suitable for studying macrophage activation in bacterial environments, future studies employing primary or human immune cells will be required to further support the translational relevance of these findings. In addition, biofilm formation was assessed using the well-established biofilm-forming *Staphylococcus epidermidis* strain RP62A; although our results are highly promising, investigations including additional clinically relevant strains such as *Staphylococcus aureus* are needed to confirm the general applicability of the observed effects. Furthermore, macrophage activation was evaluated using biofilm-derived supernatants rather than direct cell–material–bacteria interaction models, which may not fully capture the complexity of in vivo conditions. Finally, the underlying mechanisms responsible for the observed reduction in biofilm formation by BG could not be fully elucidated within the scope of this study and likely involve a combination of ion release, local pH changes and

surface-related features. In addition, long-term performance aspects, including coating durability under mechanical loading, ion release stability and maintenance of anti-bacterial activity under physiological conditions, were not addressed and require further investigation to support clinical translation.

5. Conclusions

To date, no bioactive glass coated implants are clinically available for revision arthroplasty, a procedure associated with a high risk of infection. In this study, 45S5-BG coatings on Ti-6Al-4V alloys demonstrated a significant reduction in biofilm formation of *Staphylococcus epidermidis* compared to state-of-the-art HA, accompanied by an increase in local pH, while maintaining comparable host cell viability and morphology. Importantly, BG coatings preserved antibacterial macrophage activation and promoted a more pronounced M1-like phenotype under biofilm-associated conditions, suggesting that antibacterial immune defense is not impaired. Together, these findings indicate that BG coatings achieve a favorable balance between cytocompatibility and antibacterial performance. While the translational potential of these findings is promising, further validation is required, including in vivo studies and investigations under clinically relevant conditions.

Overall, our findings highlight the potential of 45S5-BG coatings as a multifunctional surface modification strategy that, in contrast to conventional HA coatings, not only supports host cell compatibility but also actively contributes to antibacterial defense. This dual functionality represents a promising approach for improving implant performance in infection-prone revision arthroplasty.

CRediT authorship contribution statement

Elisabeth Seebach: Writing – review & editing, Writing – original draft, Validation, Methodology, Investigation, Formal analysis, Conceptualization. **Jan Philippe Kretzer:** Validation, Methodology, Investigation. **Therese Bormann:** Validation, Investigation. **Jens Gibmeier:** Writing – original draft, Validation, Methodology, Investigation. **Robert Vaßen:** Validation, Methodology, Investigation, Formal analysis. **Elke Kunisch:** Validation, Methodology, Investigation, Formal analysis. **Tobias Renkawitz:** Validation, Resources. **Fabian Westhauser:** Writing – review & editing, Writing – original draft, Validation, Conceptualization.

Declaration of Generative AI and AI-assisted technologies in the writing process

AI-based tools were used to assist with literature discovery (Elicit) and English language editing (ChatGPT). All scientific content, interpretations and conclusions were determined by the authors.

Declaration of competing interest

The authors declare that they have no known competing financial interests or personal relationships that could have appeared to influence the work reported in this paper.

Acknowledgements

The authors thank Anna-Lena Otte for support with the SEM analysis of the coatings. This research did not receive any specific grant from funding agencies in the public, commercial, or not-for-profit sectors. The graphical abstract was created in BioRender (Seebach, E. (2026) https://BioRender.com/74mlcsl).

Appendix A. Supplementary data

Supplementary data to this article can be found online at https://doi.org/10.1016/j.bioadv.2026.214895.

Data availability

Data will be made available on request.

References

[1] J. Parvizi, B. Adeli, B. Zmistowski, C. Restrepo, A.S. Greenwald, Management of periprosthetic joint infection: the current knowledge: AAOS exhibit selection, J. Bone Joint Surg. Am. 94 (2012) e104, https://doi.org/10.2106/jbjs.K.01417.
[2] B. Zmistowski, J.A. Karam, J.B. Durinka, D.S. Casper, J. Parvizi, Periprosthetic joint infection increases the risk of one-year mortality, J. Bone Joint Surg. Am. 95 (2013) 2177–2184, https://doi.org/10.2106/jbjs.L.00789.
[3] J.-H. Baek, S.C. Lee, H. Jin, J.-W. Kim, H.S. Ahn, C.H. Nam, Poor outcomes of revision total knee arthroplasty in patients with septic loosening compared to patients with aseptic loosening, J. Orthop. Surg. Res. 16 (2021) 624, https://doi.org/10.1186/s13018-021-02766-y.
[4] S.M. Jafari, C. Coyle, S.M.J. Mortazavi, P.F. Sharkey, J. Parvizi, Revision hip arthroplasty: infection is the most common cause of failure, Clin. Orthop. Relat. Res. 468 (2010) 2046–2051, https://doi.org/10.1007/s11999-010-1251-6.
[5] A. Grimberg, J. Lützner, O. Melsheimer, M. Morlock, A. Steinbrück, The German Arthroplasty Registry (EPRD): Annual Report, 2023.
[6] J.J. Prokopetz, E. Losina, R.L. Bliss, J. Wright, J.A. Baron, J.N. Katz, Risk factors for revision of primary total hip arthroplasty: a systematic review, BMC Musculoskelet. Disord. 13 (2012) 251, https://doi.org/10.1186/1471-2474-13-251.
[7] S. Marmor, Y. Kerroumi, Patient-specific risk factors for infection in arthroplasty procedure, Orthop. Traumatol. Surg. Res. 102 (2016) S113–S119, https://doi.org/10.1016/j.otsr.2015.05.012.
[8] R.B. da Silva, M.J. Salles, Outcomes and risk factors in prosthetic joint infections by multidrug-resistant gram-negative bacteria: a retrospective cohort study, Antibiotics (Basel) 10 (2021), https://doi.org/10.3390/antibiotics10030340.
[9] E. Garcia-Cimbrelo, E. Garcia-Rey, A. Cruz-Pardos, The extent of the bone defect affects the outcome of femoral reconstruction in revision surgery with impacted bone grafting: a five- to 17-year follow-up study, J. Bone Joint Surg. (Br.) 93 (2011) 1457–1464, https://doi.org/10.1302/0301-620x.93b11.27321.
[10] E. Zhang, X. Zhao, J. Hu, R. Wang, S. Fu, G. Qin, Antibacterial metals and alloys for potential biomedical implants, Bioact. Mater. 6 (2021) 2569–2612, https://doi.org/10.1016/j.bioactmat.2021.01.030.
[11] J. Sui, S. Liu, M. Chen, H. Zhang, Surface bio-functionalization of anti-bacterial titanium implants: a review, Coatings 12 (2022) 1125.
[12] X. Chen, J. Zhou, Y. Qian, L. Zhao, Antibacterial coatings on orthopedic implants, Mater. Today Bio 19 (2023) 100586, https://doi.org/10.1016/j.mtbio.2023.100586.
[13] J.-a.N. Oliver, Y. Su, X. Lu, P.-H. Kuo, J. Du, D. Zhu, Bioactive glass coatings on metallic implants for biomedical applications, Bioact. Mater. 4 (2019) 261–270, https://doi.org/10.1016/j.bioactmat.2019.09.002.
[14] L.L. Hench, Chronology of bioactive glass development and clinical applications, New J. Glass Ceram. 3 (2013) 67–73, https://doi.org/10.4236/njgc.2013.32011.
[15] D.C. Greenspan, Bioactive glass: mechanisms of bone bonding, Tandläkartidningen Ark 91 (1999) 1–32.
[16] I.D. Xynos, A.J. Edgar, L.D. Buttery, L.L. Hench, J.M. Polak, Gene-expression profiling of human osteoblasts following treatment with the ionic products of Bioglass 45S5 dissolution, J. Biomed. Mater. Res. 55 (2001) 151–157, https://doi.org/10.1002/1097-4636(200105)55:2<151::aid-jbm1001>3.0.co;2-d.
[17] L.L. Hench, The story of Bioglass, J. Mater. Sci. Mater. Med. 17 (2006) 967–978, https://doi.org/10.1007/s10856-006-0432-z.
[18] J.R. Jones, Review of bioactive glass: from Hench to hybrids, Acta Biomater. 9 (2013) 4457–4486, https://doi.org/10.1016/j.actbio.2012.08.023.
[19] S. Hu, J. Chang, M. Liu, C. Ning, Study on antibacterial effect of 45S5 Bioglass, J. Mater. Sci. Mater. Med. 20 (2009) 281–286, https://doi.org/10.1007/s10856-008-3564-5.
[20] E. Kunisch, L.A. Fiehn, M. Saur, M. Arango-Ospina, C. Merle, S. Hagmann, A. Stiller, L. Hupa, T. Renkawitz, A.R. Boccaccini, F. Westhauser, A comparative in vitro and in vivo analysis of the biological properties of the 45S5-, 1393-, and 0106-B1-bioactive glass compositions using human bone marrow-derived stromal cells and a rodent critical size femoral defect model, Biomater. Adv. 153 (2023) 213521, https://doi.org/10.1016/j.bioadv.2023.213521.
[21] F.E. Ciraldo, E. Boccardi, V. Melli, F. Westhauser, A.R. Boccaccini, Tackling bioactive glass excessive in vitro bioreactivity: preconditioning approaches for cell culture tests, Acta Biomater. 75 (2018) 3–10, https://doi.org/10.1016/j.actbio.2018.05.019.
[22] Q. Nawaz, A. de Pablos-Martín, J. Martins de Souza e Silva, K. Hurle, A.T. C. Jaimes, D.S. Brauer, A.R. Boccaccini, New insights into the crystallization process of sol-gel–derived 45S5 bioactive glass, J. Am. Ceram. Soc. 103 (2020) 4234–4247, https://doi.org/10.1111/jace.17124.
[23] G. Kaur, V. Kumar, F. Baino, J.C. Mauro, G. Pickrell, I. Evans, O. Bretcanu, Mechanical properties of bioactive glasses, ceramics, glass-ceramics and composites: state-of-the-art review and future challenges, Mater. Sci. Eng. C 104 (2019) 109895, https://doi.org/10.1016/j.msec.2019.109895.
[24] P. Xin, J. Yang, G. Chen, Y. Wang, Y. Wang, G. Zhang, Clinical and radiographic outcomes of long monoblock, hydroxyapatite-coated stem in revision hip arthroplasty with extended trochanteric osteotomy: a multicenter study, J. Orthop. Surg. Res. 19 (2024) 20, https://doi.org/10.1186/s13018-023-04377-1.

[25] T.J. Wood, M. Alzahrani, D. Marsh, L.E. Somerville, E.M. Vasarhelyi, B.A. Lanting, Use of the Corail stem for revision total hip arthroplasty: evaluation of clinical outcomes and cost, Can. J. Surg. 62 (2019) 78–82, https://doi.org/10.1503/cjs.002318.
[26] T.M. Lee, E.Y. Chang, B.-C. Wang, C.-y. Yang, Characteristics of plasma-sprayed bioactive glass coatings on Ti-6A1-4V alloy: an in vitro study, Surf. Coat. Technol. 79 (1996) 170–177, https://doi.org/10.1016/0257-8972(95)02463-8.
[27] V. López Calvo, M. Vicent Cabedo, E. Bannier, E. Cañas Recacha, A.R. Boccaccini, L. Cordero Arias, E. Sánchez Vilches, 45S5 bioactive glass coatings by atmospheric plasma spraying obtained from feedstocks prepared by different routes, J. Mater. Sci. 49 (2014) 7933–7942, https://doi.org/10.1007/s10853-014-8519-2.
[28] B. Widholz, S. Tsitlakidis, B. Reible, A. Moghaddam, F. Westhauser, Pooling of patient-derived mesenchymal stromal cells reduces inter-individual confounder-associated variation without negative impact on cell viability, proliferation and osteogenic differentiation, Cells 8 (2019), https://doi.org/10.3390/cells8060633.
[29] A.E. Carpenter, T.R. Jones, M.R. Lamprecht, C. Clarke, I.H. Kang, O. Friman, D. A. Guertin, J.H. Chang, R.A. Lindquist, J. Moffat, P. Golland, D.M. Sabatini, CellProfiler: image analysis software for identifying and quantifying cell phenotypes, Genome Biol. 7 (2006) R100, https://doi.org/10.1186/gb-2006-7-10-r100.
[30] G.D. Christensen, W.A. Simpson, J.J. Younger, L.M. Baddour, F.F. Barrett, D. M. Melton, E.H. Beachey, Adherence of coagulase-negative Staphylococci to plastic tissue culture plates: a quantitative model for the adherence of Staphylococci to medical devices, J. Clin. Microbiol. 22 (1985) 996–1006, https://doi.org/10.1128/jcm.22.6.996-1006.1985.
[31] S. Chen, A. Saeed, Q. Liu, Q. Jiang, H. Xu, G.G. Xiao, L. Rao, Y. Duo, Macrophages in immunoregulation and therapeutics, Signal Transduct. Target. Ther. 8 (2023) 207, https://doi.org/10.1038/s41392-023-01452-1.
[32] C.G. Peace, L.A. O'Neill, The role of itaconate in host defense and inflammation, J. Clin. Invest. 132 (2022), https://doi.org/10.1172/JCI148548.
[33] P. Zhou, B.L. Garcia, G.A. Kotsakis, Comparison of antibacterial and antibiofilm activity of bioactive glass compounds S53P4 and 45S5, BMC Microbiol. 22 (2022) 212, https://doi.org/10.1186/s12866-022-02617-8.
[34] L. Drago, M. Toscano, M. Bottagisio, Recent evidence on bioactive glass antimicrobial and antibiofilm activity: a mini-review, Materials (Basel) 11 (2018) 326, https://doi.org/10.3390/ma11020326.
[35] D. Tejero-Martin, M.R. Rad, A. McDonald, T. Hussain, Beyond traditional coatings: a review on thermal-sprayed functional and smart coatings, J. Therm. Spray Technol. 28 (2019) 598–644, https://doi.org/10.1007/s11666-019-00857-1.
[36] B. Garrido, N. Garcia-Giralt, M.A. Rodriguez, A.H. de Aza, I.G. Cano, Bioactive glasses as alternatives to hydroxyapatite for bone implant coatings: a comparative study, J Biomed Mater Res B Appl Biomater 113 (2025) e35577, https://doi.org/10.1002/jbm.b.35577.
[37] F. Westhauser, M. Arango-Ospina, L. Hupa, T. Renkawitz, A.R. Boccaccini, E. Kunisch, A comparative analysis of the cytocompatibility, protein adsorption, osteogenic and angiogenic properties of the 45S5- and S53P4-bioactive glass compositions, Biomed. Mater. 19 (2024), https://doi.org/10.1088/1748-605X/ad2210.
[38] S. Wilkesmann, J. Fellenberg, Q. Nawaz, B. Reible, A. Moghaddam, A. R. Boccaccini, F. Westhauser, Primary osteoblasts, osteoblast precursor cells or osteoblast-like cell lines: which human cell types are (most) suitable for characterizing 45S5-bioactive glass? J. Biomed. Mater. Res. A 108 (2020) 663–674, https://doi.org/10.1002/jbm.a.36846.
[39] R. Detsch, S. Alles, J. Hum, P. Westenberger, F. Sieker, D. Heusinger, C. Kasper, A. R. Boccaccini, Osteogenic differentiation of umbilical cord and adipose derived stem cells onto highly porous 45S5 Bioglass(R)-based scaffolds, J. Biomed. Mater. Res. A 103 (2015) 1029–1037, https://doi.org/10.1002/jbm.a.35238.
[40] C. Rodrigues, L.I.S. Naasani, C. Zanatelli, T.C. Paim, J.G. Azevedo, J.C. de Lima, M. da Cruz Fernandes, S. Buchner, M.R. Wink, Bioglass 45S5: structural characterization of short range order and analysis of biocompatibility with adipose-derived mesenchymal stromal cells in vitro and in vivo, Mater. Sci. Eng. C Mater. Biol. Appl. 103 (2019) 109781, https://doi.org/10.1016/j.msec.2019.109781.
[41] B.L. Banik, T.R. Riley, C.J. Platt, J.L. Brown, Human mesenchymal stem cell morphology and migration on microtextured titanium, Front. Bioeng. Biotechnol. 4 (2016), https://doi.org/10.3389/fbioe.2016.00041.
[42] E.G. Long, M. Buluk, M.B. Gallagher, J.M. Schneider, J.L. Brown, Human mesenchymal stem cell morphology, migration, and differentiation on micro and nano-textured titanium, Bioact. Mater. 4 (2019) 249–255, https://doi.org/10.1016/j.bioactmat.2019.08.001.
[43] H. Osman, F. Wang, G. Zou, D. Zhang, X. Bai, T. Jiang, Y. Wang, Antibacterial and osteogenic gain strategy on titanium surfaces for preventing implant-related infections, Colloids Surf. B: Biointerfaces 249 (2025) 114489, https://doi.org/10.1016/j.colsurfb.2024.114489.
[44] S. Kowalski, W. Gonciarz, R. Belka, A. Góral, M. Chmiela, L. Lechowicz, W. Kaca, W. Zórawski, Plasma-sprayed hydroxyapatite coatings and their biological properties, Coatings 12 (2022), https://doi.org/10.3390/coatings12091317.
[45] D.C. Coraca-Huber, M. Fille, J. Hausdorfer, D. Putzer, M. Nogler, Efficacy of antibacterial bioactive glass S53P4 against S. aureus biofilms grown on titanium discs in vitro, J. Orthop. Res. 32 (2014) 175–177, https://doi.org/10.1002/jor.22463.
[46] M. Bortolin, E. De Vecchi, C.L. Romanò, M. Toscano, R. Mattina, L. Drago, Antibiofilm agents against MDR bacterial strains: is bioactive glass BAG-S53P4 also effective? J. Antimicrob. Chemother. 71 (2016) 123–127, https://doi.org/10.1093/jac/dkv327.
[47] L. Drago, C. Vassena, S. Fenu, E. De Vecchi, V. Signori, R. De Francesco, C. L. Romanò, Antibiofilm activity of bioactive glass S53P4, Future Microbiol. 9 (2014) 593–601, https://doi.org/10.2217/fmb.14.20.
[48] S. Begum, W.E. Johnson, T. Worthington, R.A. Martin, The influence of pH and fluid dynamics on the antibacterial efficacy of 45S5 Bioglass, Biomed. Mater. 11 (2016) 015006, https://doi.org/10.1088/1748-6041/11/1/015006.
[49] D.P. Linklater, V.A. Baulin, S. Juodkazis, R.J. Crawford, P. Stoodley, E.P. Ivanova, Mechano-bactericidal actions of nanostructured surfaces, Nat. Rev. Microbiol. 19 (2021) 8–22, https://doi.org/10.1038/s41579-020-0414-z.
[50] N.P. Boks, H.J. Kaper, W. Norde, H.C. van der Mei, H.J. Busscher, Mobile and immobile adhesion of staphylococcal strains to hydrophilic and hydrophobic surfaces, J. Colloid Interface Sci. 331 (2009) 60–64, https://doi.org/10.1016/j.jcis.2008.11.025.
[51] N. Cerca, G.B. Pier, M. Vilanova, R. Oliveira, J. Azeredo, Quantitative analysis of adhesion and biofilm formation on hydrophilic and hydrophobic surfaces of clinical isolates of Staphylococcus epidermidis, Res. Microbiol. 156 (2005) 506–514, https://doi.org/10.1016/j.resmic.2005.01.007.
[52] A. Nostro, L. Cellini, M. Di Giulio, M. D'Arrigo, A. Marino, A.R. Blanco, A. Favaloro, G. Cutroneo, G. Bisignano, Effect of alkaline pH on staphylococcal biofilm formation, APMIS 120 (2012) 733–742, https://doi.org/10.1111/j.1600-0463.2012.02900.x.
[53] S. Tsitlakidis, F. Hohenbild, M. Saur, A. Moghaddam, E. Kunisch, T. Renkawitz, I. Gonzalo de Juan, F. Westhauser, Reduced sodium portions favor osteogenic properties and cytocompatibility of 45S5-based bioactive glass particles, Biomimetics (Basel) 8 (2023), https://doi.org/10.3390/biomimetics8060472.
[54] Lei Wang, C.Y. Fan Wang, Qiang Wang, Degang Huang, Xin Yang, Tao Ma, Pingbo Chen, Congming Li, Zhouzhou Zhang, Guoyang Wan, Xing Yang, Bioactive manganese-decorated titanium implants for osteoporotic bone regeneration, Mater. Today Adv. 24 (2024), https://doi.org/10.1016/j.mtadv.2024.100542.
[55] R.M. Day, A.R. Boccaccini, Effect of particulate bioactive glasses on human macrophages and monocytes in vitro, J. Biomed. Mater. Res. A 73 (2005) 73–79, https://doi.org/10.1002/jbm.a.30262.
[56] K. Kajander, N. Nowak, N. Vaziri, P.K. Vallittu, T.J. Heino, J.A. Määttä, Unraveling the immunomodulatory and metabolic effects of bioactive glass S53P4 on macrophages in vitro, J. Mater. Sci.-Mater. Med. 36 (2025), https://doi.org/10.1007/s10856-025-06861-y.
[57] E. Seebach, T. Elschner, F.V. Kraus, M. Souto-Carneiro, K.F. Kubatzky, Bacterial and metabolic factors of staphylococcal planktonic and biofilm environments differentially regulate macrophage immune activation, Inflammation 46 (2023) 1512–1530, https://doi.org/10.1007/s10753-023-01824-3.
[58] M. Benoit, B. Desnues, J.-L. Mege, Macrophage polarization in bacterial infections, J. Immunol. 181 (2008) 3733–3739, https://doi.org/10.4049/jimmunol.181.6.3733.
[59] K.Y. Lee, M1 and M2 polarization of macrophages: a mini-review, Med. Biol. Sci. Eng. 2 (2019) 1–5, https://doi.org/10.30579/mbse.2019.2.1.1.
[60] E. Seebach, K.F. Kubatzky, Chronic implant-related bone infections-can immune modulation be a therapeutic strategy? Front. Immunol. 10 (2019) 1724, https://doi.org/10.3389/fimmu.2019.01724.
[61] K.J. Yamada, C.E. Heim, X. Xi, K.S. Attri, D. Wang, W. Zhang, P.K. Singh, T. K. Bronich, T. Kielian, Monocyte metabolic reprogramming promotes pro-inflammatory activity and Staphylococcus aureus biofilm clearance, PLoS Pathog. 16 (2020) e1008354, https://doi.org/10.1371/journal.ppat.1008354.
[62] C.M. Gries, T.L. Kielian, Staphylococcal biofilms and immune polarization during prosthetic joint infection, J. Am. Acad. Orthop. Surg. 25 (2017) S20–S24.
[63] X. Bai, Y.-R. Guo, Z.-m. Zhao, X.-Y. Li, D.-Q. Dai, J.-k. Zhang, Y.-S. Li, C.-D. Zhang, Macrophage polarization in cancer and beyond: from inflammatory signaling pathways to potential therapeutic strategies, Cancer Lett 625 (2025) 217772, https://doi.org/10.1016/j.canlet.2025.217772.
[64] T. Xia, M. Zhang, W. Lei, R. Yang, S. Fu, Z. Fan, Y. Yang, T. Zhang, Advances in the role of STAT3 in macrophage polarization, Front. Immunol. 14 - 2023 (2023), https://doi.org/10.3389/fimmu.2023.1160719.